Supplementary Figures:

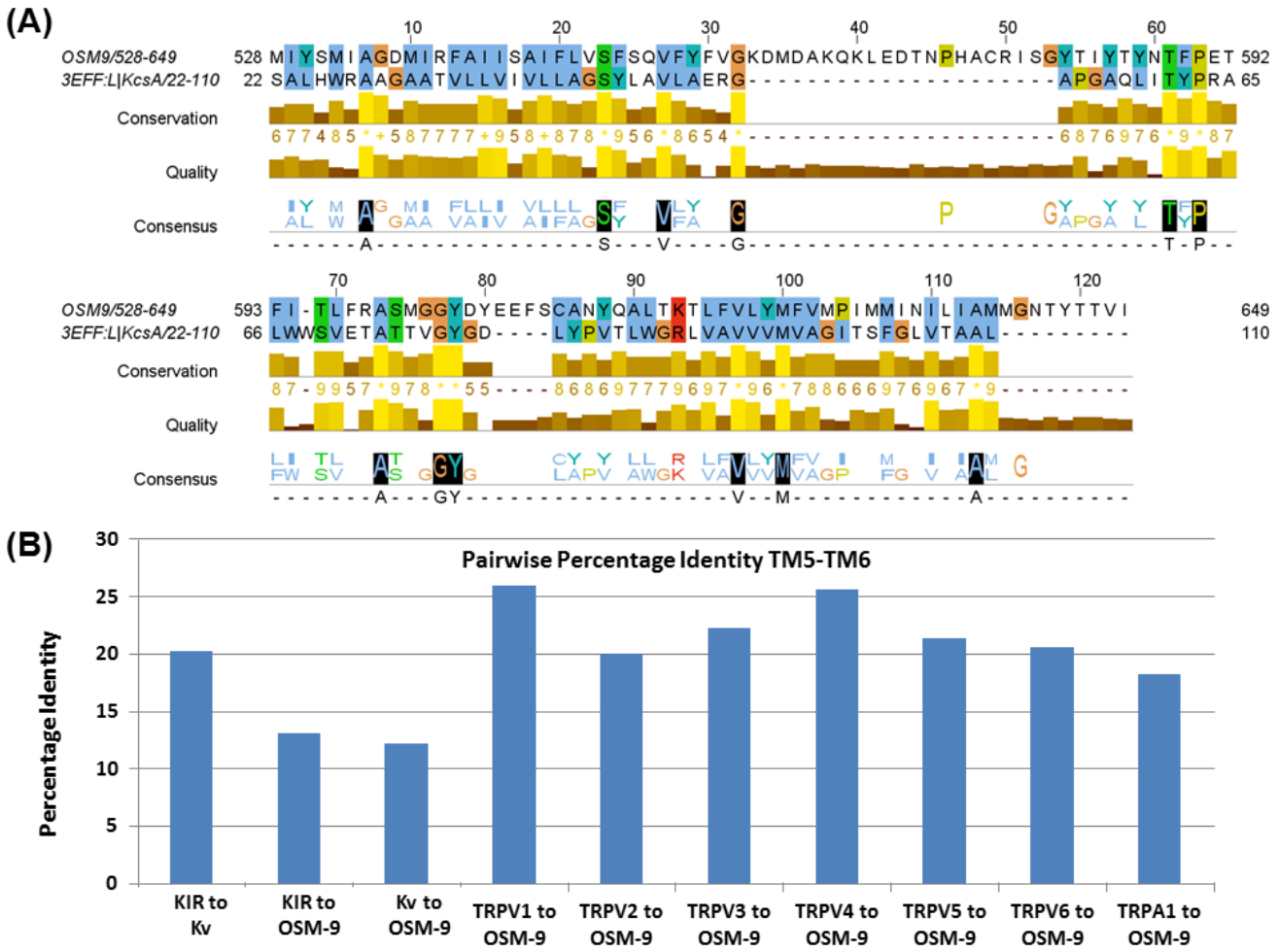

Supplementary Figure 1. Sequence similarity across pore forming unit

(A) Pairwise sequence alignment of OSM-9 TM5-TM6 and KCSA[1] was obtained from MUSCLE, manually edited by secondary structure, and colored in Jalview according to the Clustal-X sequence conservation. Sequence identity was calculated for a variety of sequence fragments: TM5-TM6, Percentage identity 10.7% (alignment length: 122 residues); Pore-Helix and Selectivity Filter, Percentage identity 26.3% (19 residues); Selectivity Filter, Percentage identity 42.9% (7 residues).

(B) Bar graph compares pairwise percentage identity between TM5-TM6 of OSM-9 versus potassium channel templates[2,3] and mouse versions of TRPV1-6.

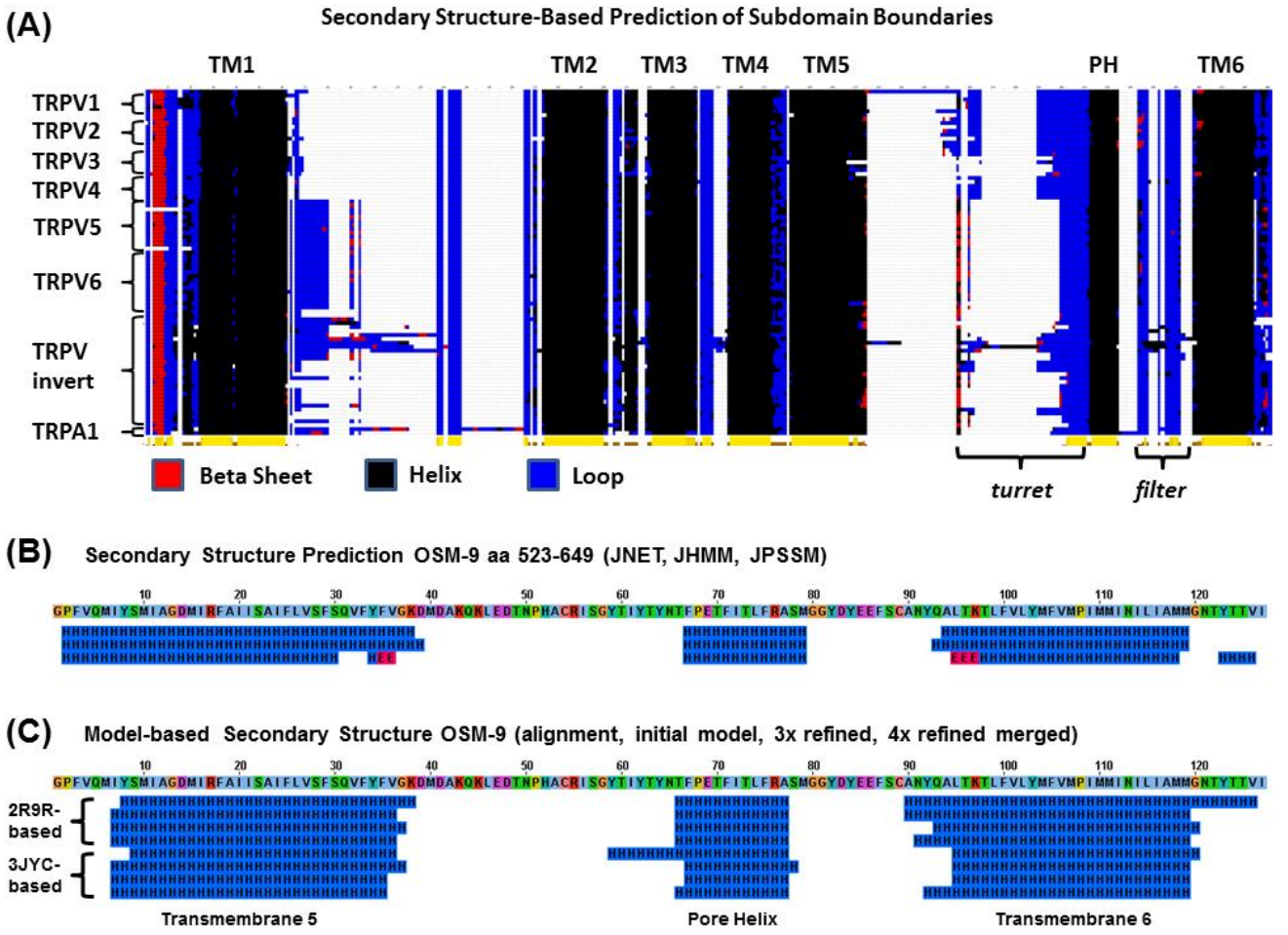

Supplementary Figure 2. Comparison of secondary structure across channel subdomains
(A) Course-grain alignment of secondary structural elements (amino acid letters encoded Helix, Extended, or Loop based on JNet prediction) in 87 TRPV sequences and one TRPA1 sequence. (B) Graphical depiction of the secondary structure prediction in the TM5-TM6 region of OSM-9 by JNET, JHMM and JPSSM. (C) Comparison of secondary structure assignment by the Kv1.2 or Kir2.2 template-based alignment, the initial structure, 3X refined, and 4X refined and merged model with their respective templates. After [2,3].

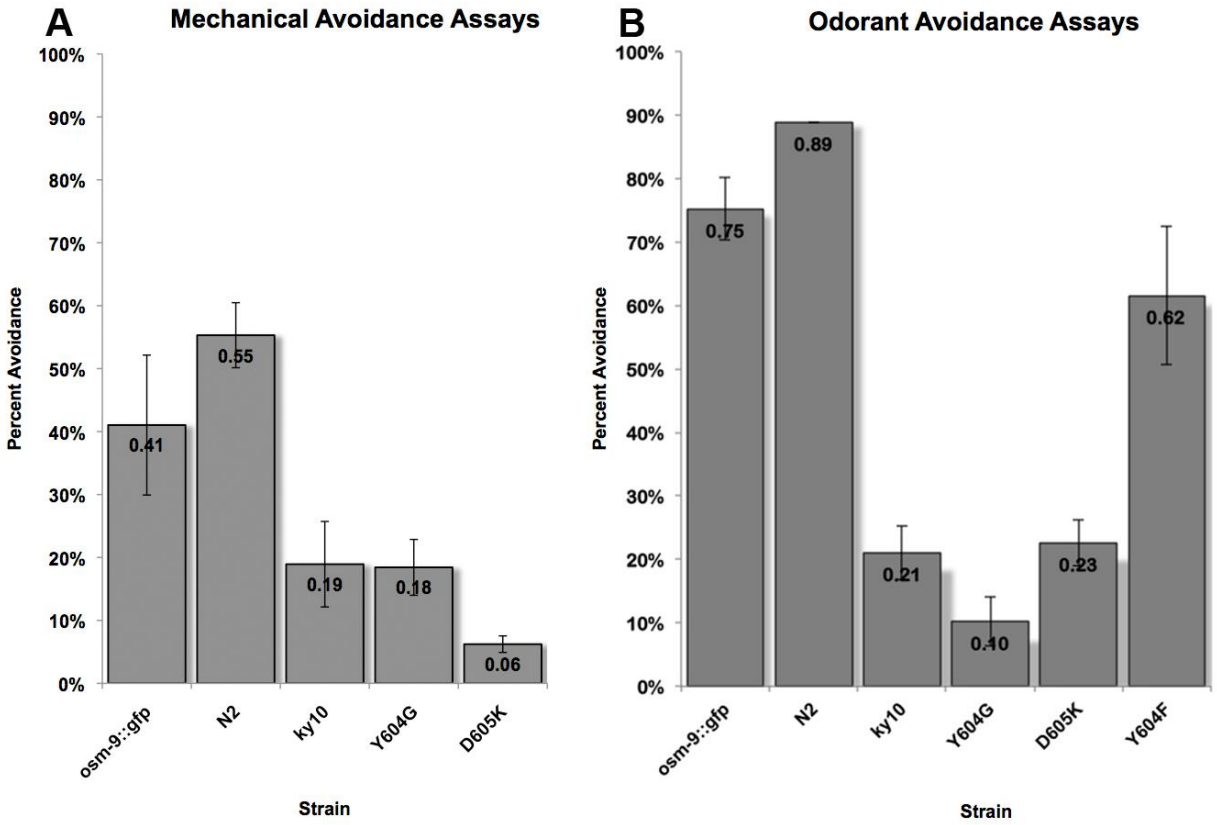

Supplementary Figure 3. Y604G, Y604F and D605K cause defects in all OSM-9 sub-modalities
(A) Y604G and D605K were defective in nose touch avoidance, equally defective as *osm-9(ky10)*. (B) Y604G and D605K were defective in odorant avoidance to similar degree as *osm-9(ky10)* worms. Bars represent mean, error bars SEM. ≥6 individual animals per line were tested, 3 lines for each strain, at 2 different time-points.

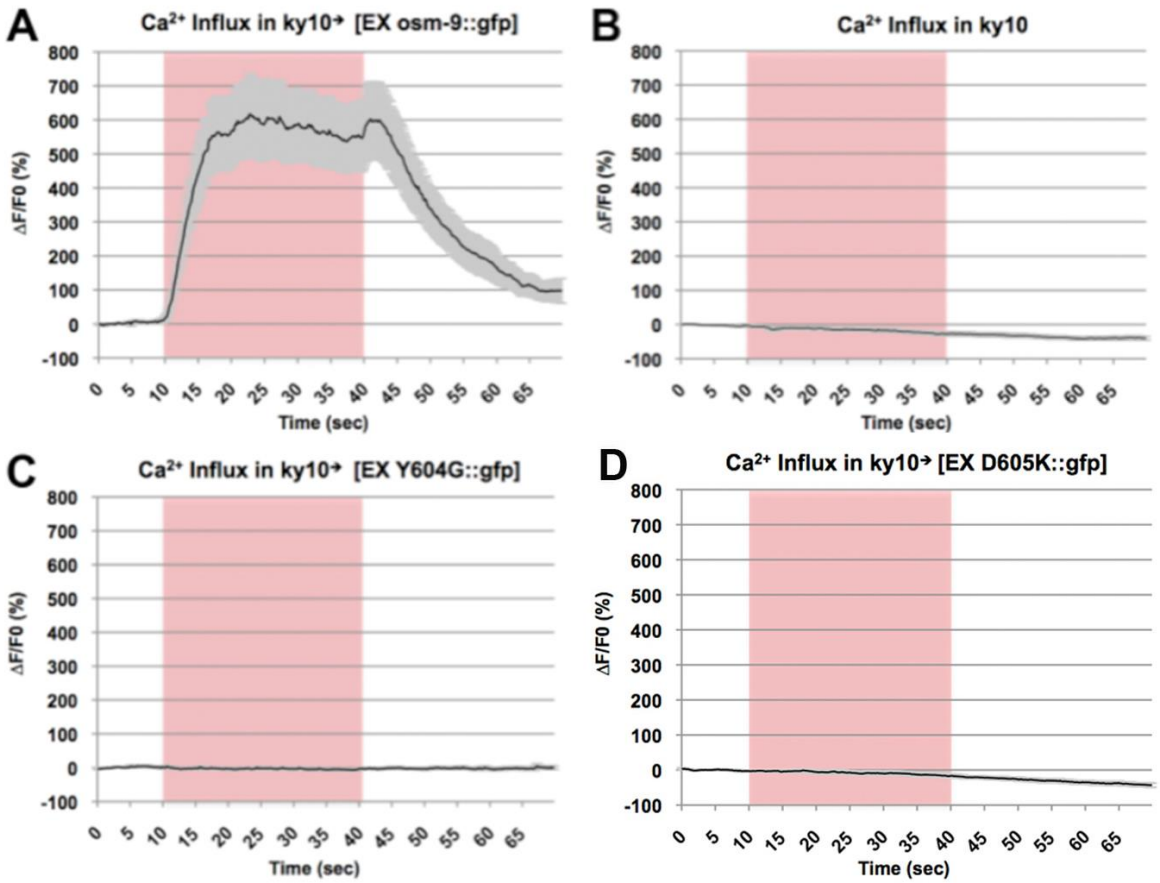

Supplementary Figure 4. Averaged Ca^{2+} transients for "dead channels", Y604G and D605K
(A-B) *osm-9::gfp* rescue and *ky10* transients shown for comparison. (C) Y604G is defective in Ca^{2+} influx and avoidance behavior (D) likewise for D605K.

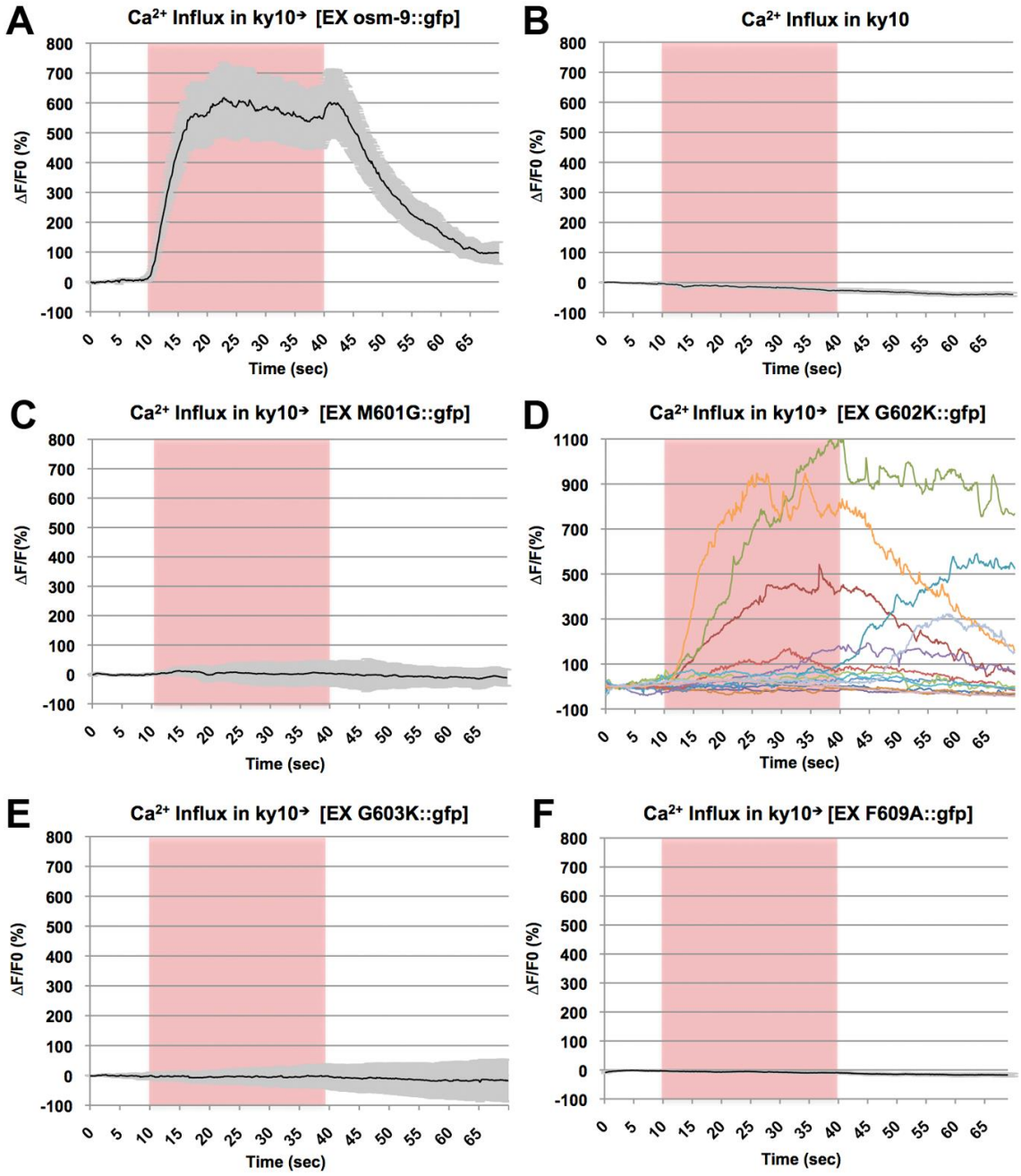

Supplementary Figure 5. Averaged Ca^{2+} transients for OSM-9 mutants partially defective in avoidance behavior

Average Ca^{2+} transients for wild-type and OSM-9 mutants that displayed partially defective osmotic avoidance behavior. (A-B) OSM-9::GFP rescue and *ky10* transients shown for comparison. (C, E, F) M601G, G603K and F609A displayed flat Ca^{2+} transients. (D) G602K displayed disrupted Ca^{2+} dynamics. Raw data is displayed, because the data was non-normal and therefore could not be averaged meaningfully.

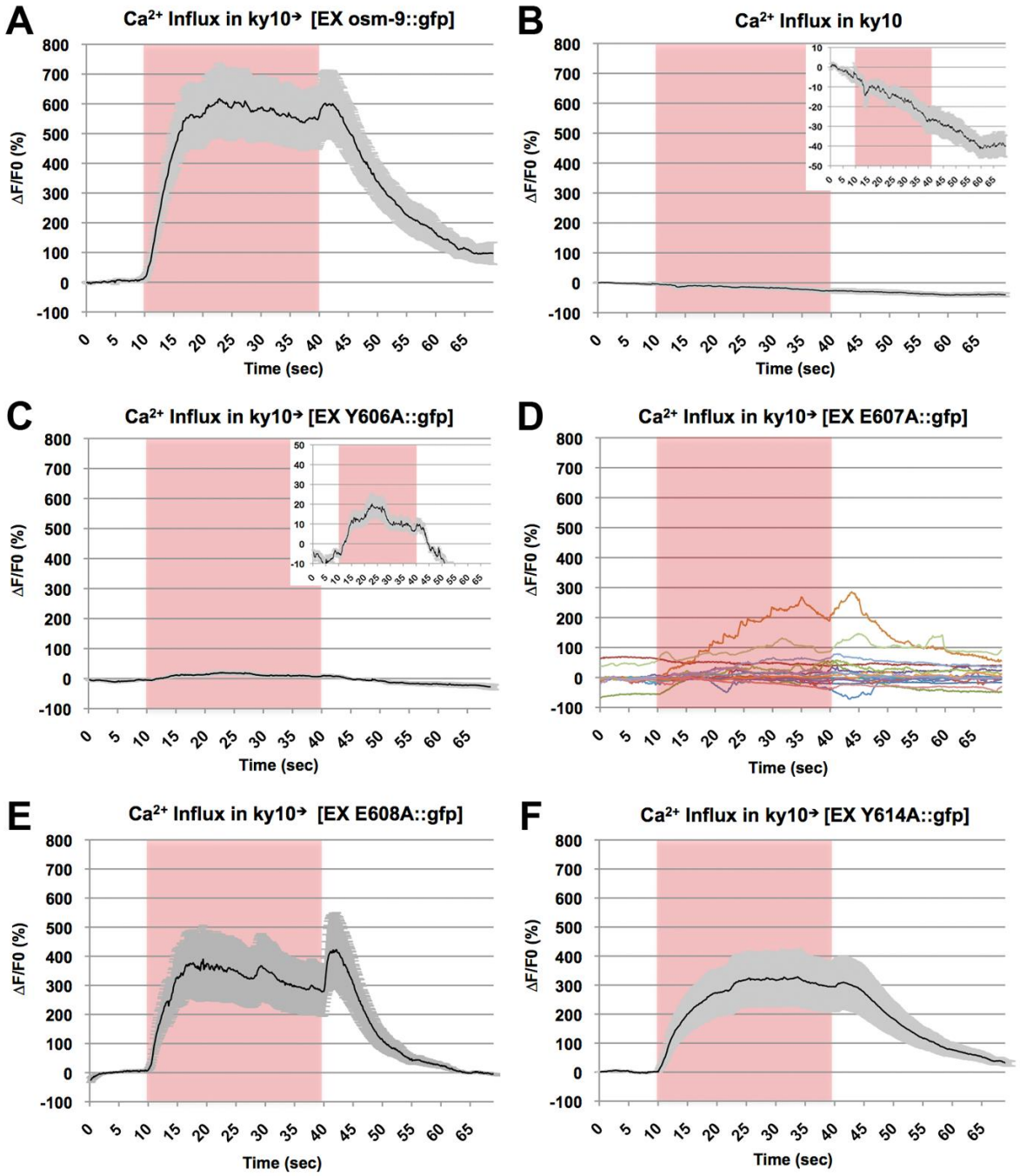

Supplementary Figure 6. Averaged Ca^{2+} transients for OSM-9 mutants wild type for avoidance behavior

Average Ca^{2+} transients for wild type and OSM-9 mutants that displayed wild-type osmotic avoidance behavior. (A-B) OSM-9::GFP rescue and *ky10* transients shown for comparison. (C-E) Y606A displays strongly reduced Ca^{2+} transients, whereas E607A displays minimal Ca^{2+} Influx, inconsistent Ca^{2+} dynamics, with nearly half of the animals tested lacking Ca^{2+} influx. E608A displays wild type patterned responses, indicating that this residue is not critical to selectivity and ion permeation. (F) Y614A served as an internal control located in the Loop 6 domain connecting the selectivity filter to TM6 of OSM-9 and shows a normal Ca^{2+} transient.

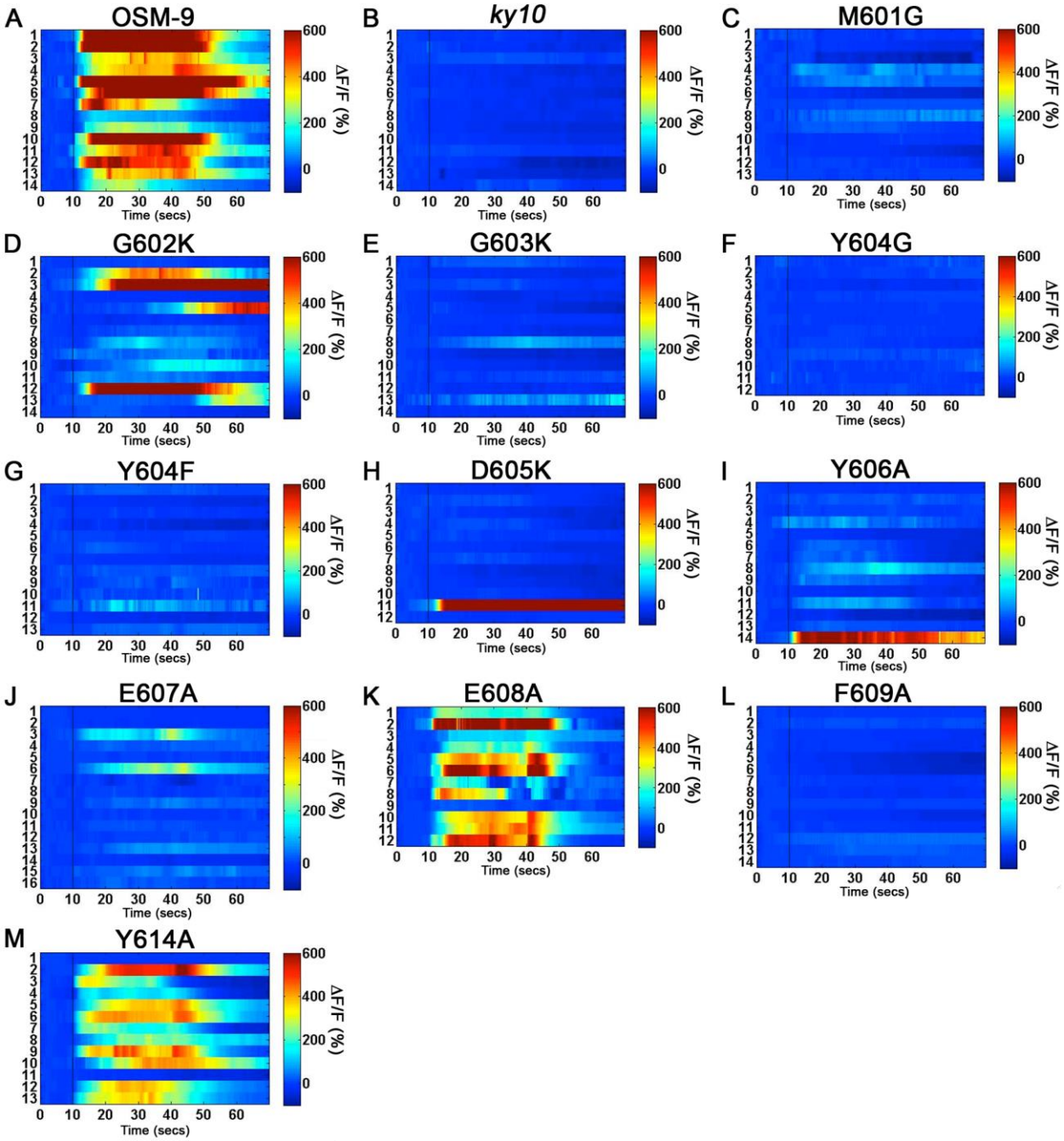

Supplementary Figure 7. Ca^{2+} transient heat maps for all OSM-9 mutants tested
(A-M) Heat maps depicting individual Ca^{2+} transients for all animals tested for each mutant strain. Trial number is on the left axis and pseudo-color index is shown on the right

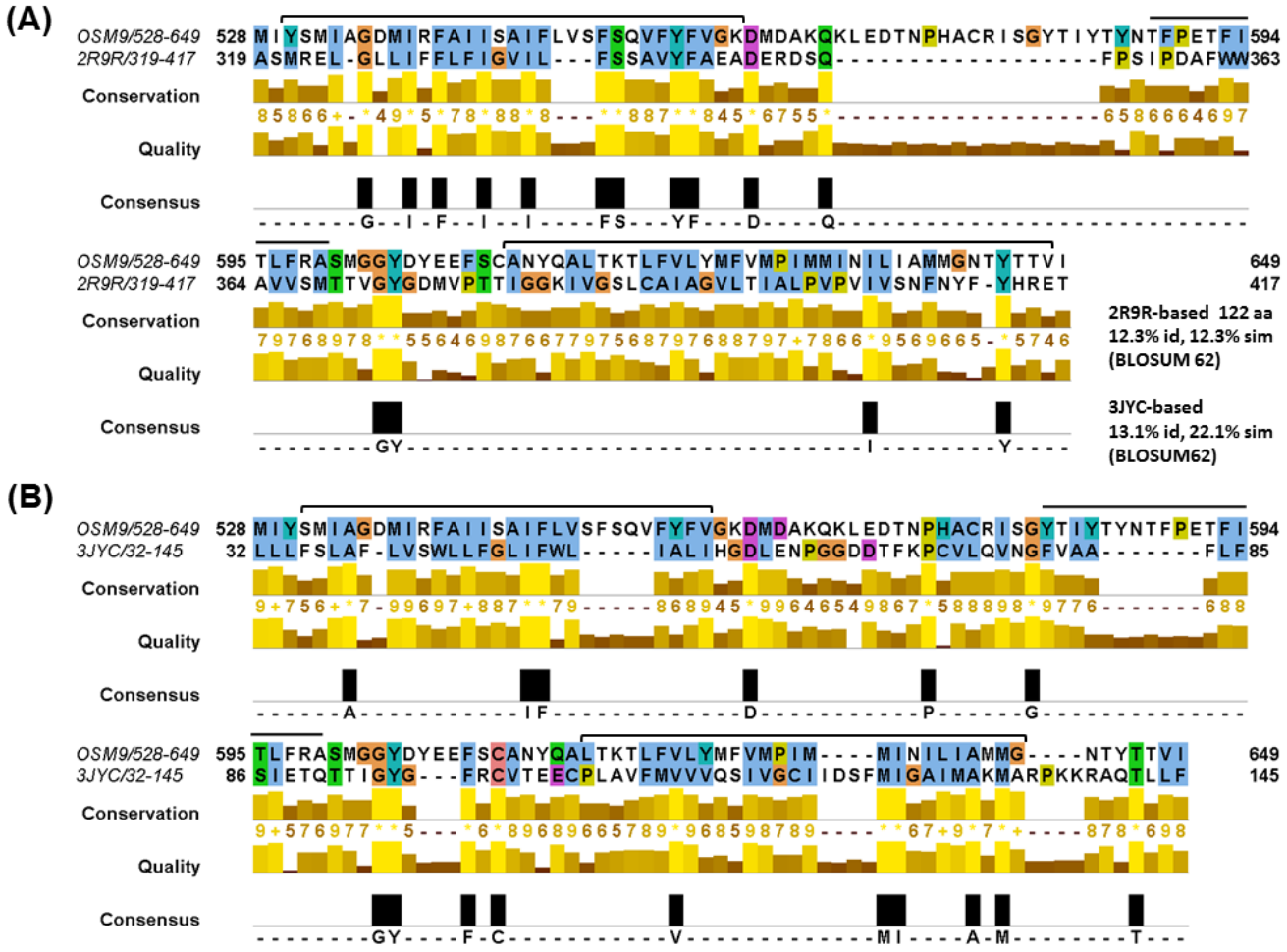

Supplementary Figure 8. Pairwise alignment for potassium channel-based homology modeling Graphical representation of pairwise alignment between OSM-9 (amino acids 528-629) with (A) Kv1.2-2.1 (amino acids 319-417, PDB ID 2R9R) or (B) with Kir2.2 (amino acids 32-145, PDB ID 3JYC). Structural boundaries from each template representing TM5, the pore helix, and TM6 are demarcated by black bars. The alignments were obtained from MUSCLE and colored in Jalview according to the Clustal-X sequence conservation. Pairwise percentage identity between Kv1.2 and OSM-9 is 12.3%; Kir2.2 and OSM-9, 13.1%; Kv1.2 and Kir2.2, 20.35%. After [2,3].

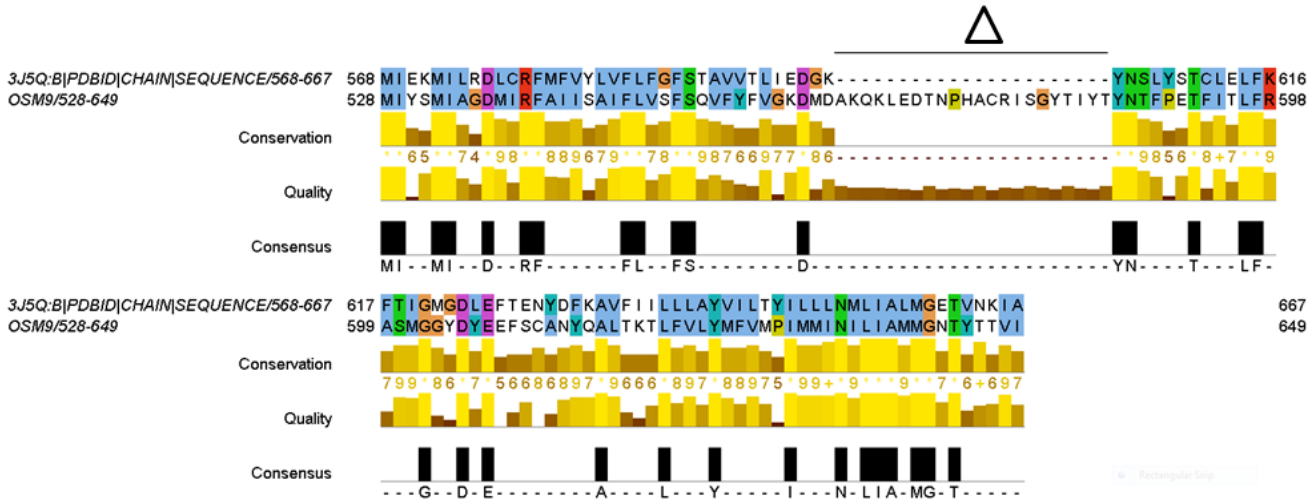

Supplementary Figure 9. Pairwise alignment for TRPV1-based homology modeling
Graphical representation of pairwise alignment between OSM-9 (amino acids 528-649) with TRPV1 (amino acids 568-667, PDB ID 3J5Q). The alignment was obtained from MUSCLE and colored in Jalview according to the Clustal-X sequence conservation. The numbering for 3J5Q is shown as contiguous but there is a shift in the atomic numbering due to the removal of the turret in 3J5Q (denoted Δ). Template/target alignments with the other two TRPV1 cryo-EM structures are identical. Pairwise percentage identity between OSM-9 and TRPV1, excluding the turret, is 31%. After [4].

(A)

INITIAL OSM-9 MODEL	molpdf	DOPE	Z-DOPE Average (SD n=30)	Z-DOPE Model	Z-DOPE Template	Procheck % (Residue regions based on Ramachandran plot) Most Favored	Allowed	Generous	Disallowed
3J5P (TRPV1)-based	*514.63*	*-13218*	*0.68 (0.14)*	*0.44*	-0.34	91	5.4	2.7	0.9
3J5Q (TRPV1)-based	666.7	-12300	1.2 (0.13)	0.973	0.716	91.9	5.4	1.8	0.9
3J5R (TRPV1)-based	755.52	-12523	1.1 (0.13)	0.844	0.583	86.5	10.8	0.9	1.8
2R9R (Kv)-based	632.15	-11588	1.3 (0.14)	1.264	-0.62	86.5	9	2.7	1.8
3JYC (Kir)-based	660.15	-10851	1.5 (0.26)	1.097	0.38	76.6	14.4	6.3	2.7

(B)

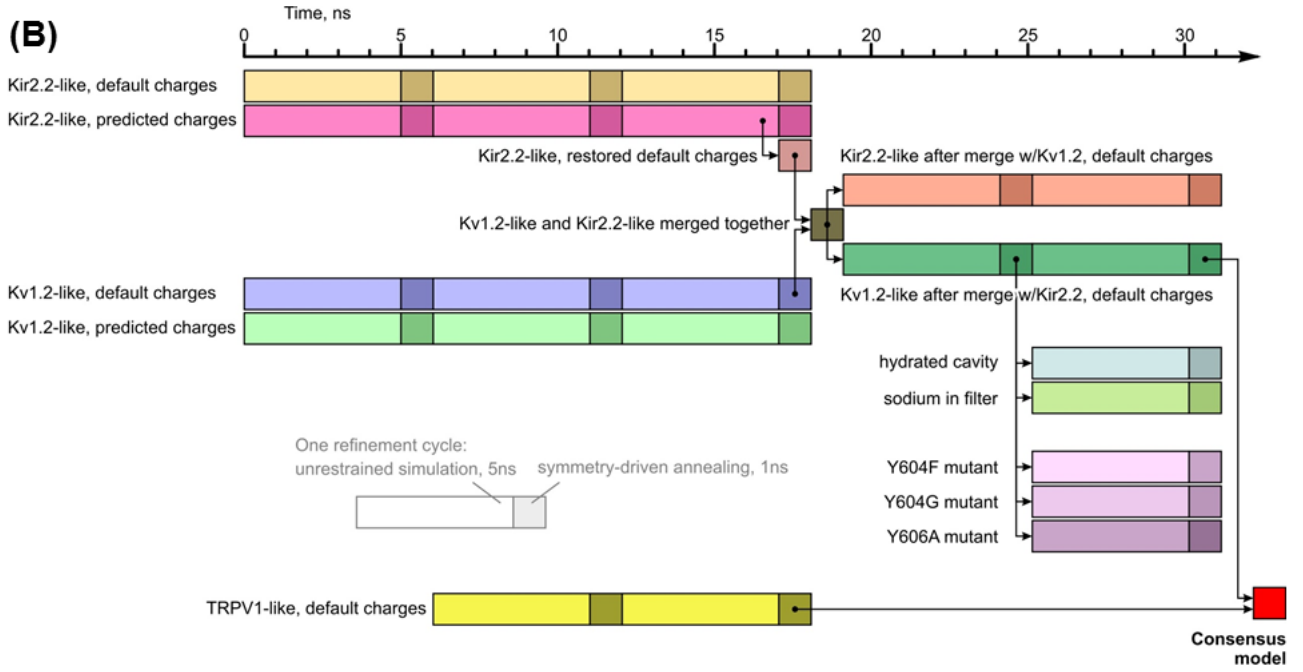

Supplementary Figure 10. Graphical representation of Molecular Dynamics refinement protocol

(A) Graphical table of various assessment scores for candidate starting models derived from structural templates[2-4]. Highlighted scores indicate candidate with 'best' score for each metric.

(B) Schematic overview of the steps involved in the MD refinement protocol for the OSM-9 structure. The protocol shows different simulation time steps carried on Kir2.2-, Kv1.2-, and TRPV1-derived models. Kir2.2- and Kv1.2- models were simulated in two variants of protonation state for certain amino acids, see Methods for complete details. To reveal and integrate the most stable features of the alternative models, after first 3 cycles of refinement for Kir2.2- and Kv1.2-like models, the best structures were converged to a continuously updating average structure, followed by 2 cycles of refinement of the merged model. The final refined Kv1.2-Kir2.2-like merged model was converged with 2x refined TRPV1-like mode following the same protocol. We also compared the wild-type Kv1.2-Kir2.2-like merged model with three mutants (Y604F, Y604G, Y606A), as well as with Na^{+} placed instead of Ca^{2+} in the selectivity filter, and with the system with fully-rehydrated ion chamber.

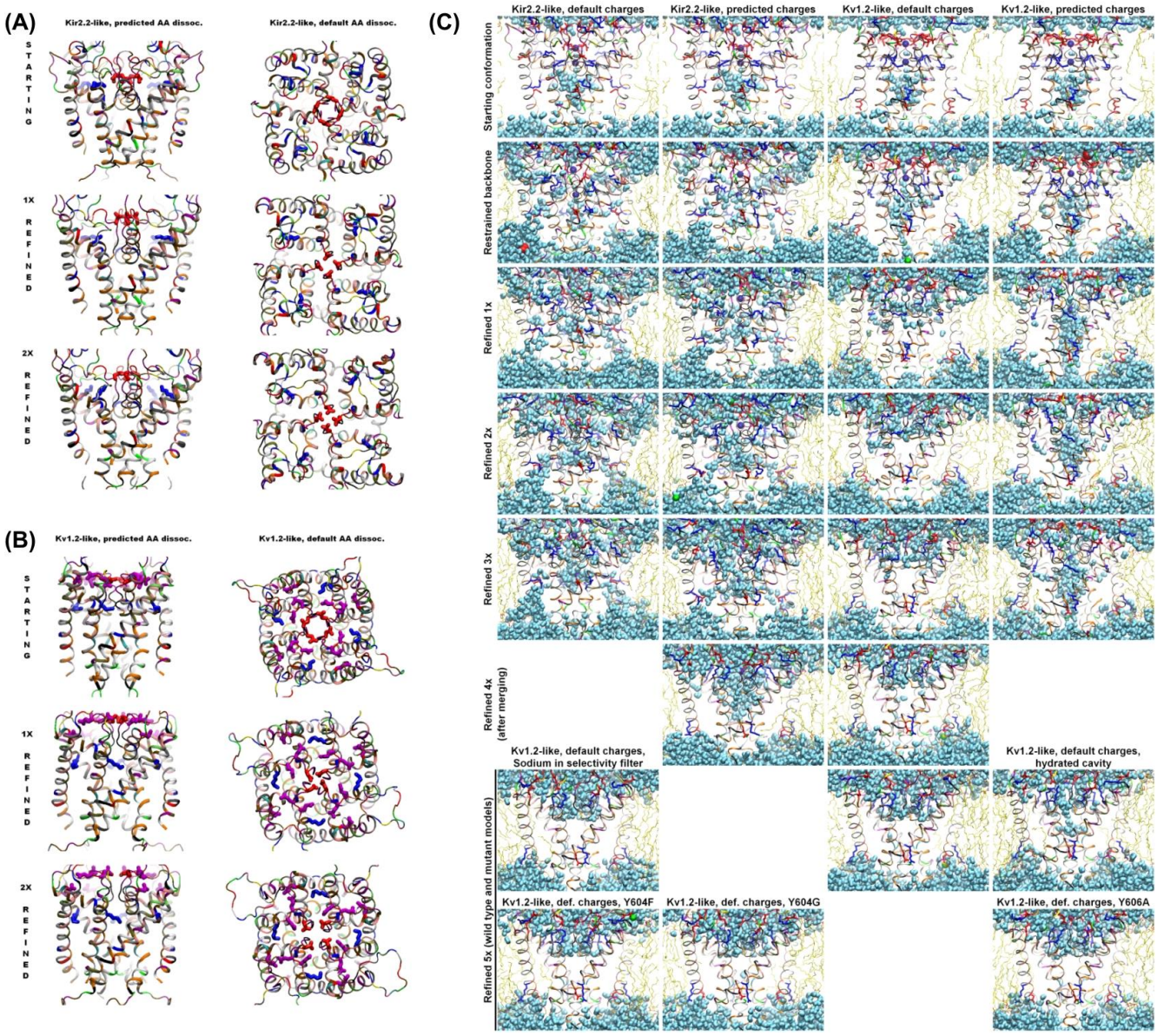

Supplementary Figure 11. Hydration evolution and refinement of Kir and Kv based structures
(A-B) Kir2.2- and Kv1.2-based models with default and predicted charges from starting structure through two cycles of refinement. The specific amino acids assessed by setting non-dissociated in predicted amino acid dissociation state were residues D^{605}, and K^{619} for Kir2.2-derived model and E^{591}, D^{605}, E^{607}, E^{608}, and K^{619} for Kv1.2-derived model. (C) Kir2.2-, Kv1.2-, and merged Kv1.2-Kir2.2-like models (wild-type and mutant) through cycles of refinement tracking protein-lipid contacts, ion coordination, and hydration states.

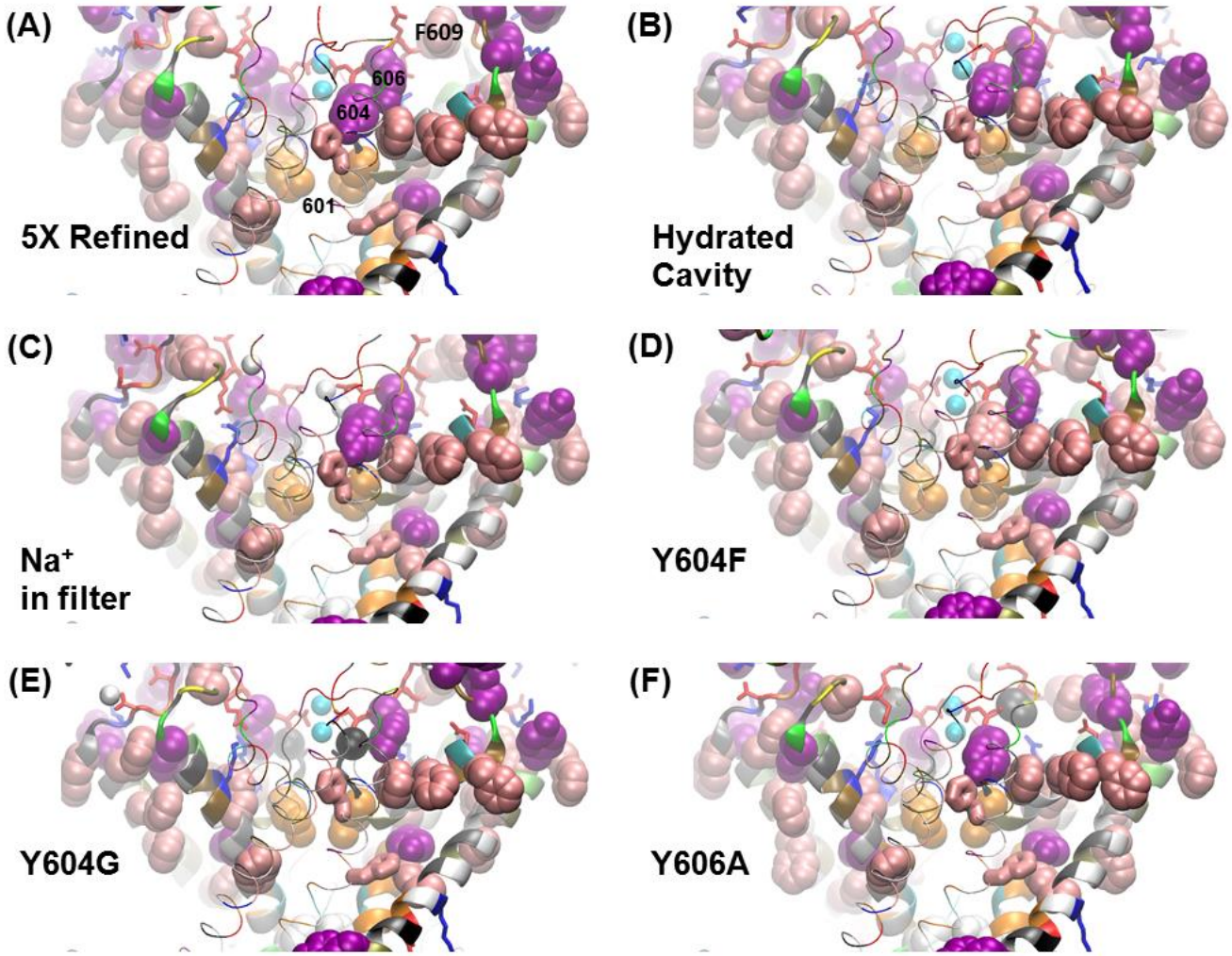

Supplementary Figure 12. Additional Kv1.2-Kir2.2-like OSM-9 models
Three mutants are shown (Y604F, Y604G, Y606A), the system with Na^+ instead of Ca^{2+}, the system with hydrated chamber and the control. Stacking in aromatic residues near the selectivity filter and the pore helix is shown. Side chains of tyrosines and phenylalanines are represented as purple and pink space fill respectively. Aromatic residues, shown as "thick licorice" rather than van der Waals are those that belong to another subunit, shown in front as thin tubes. Acidic and basic protein residues are colored red and blue respectively.

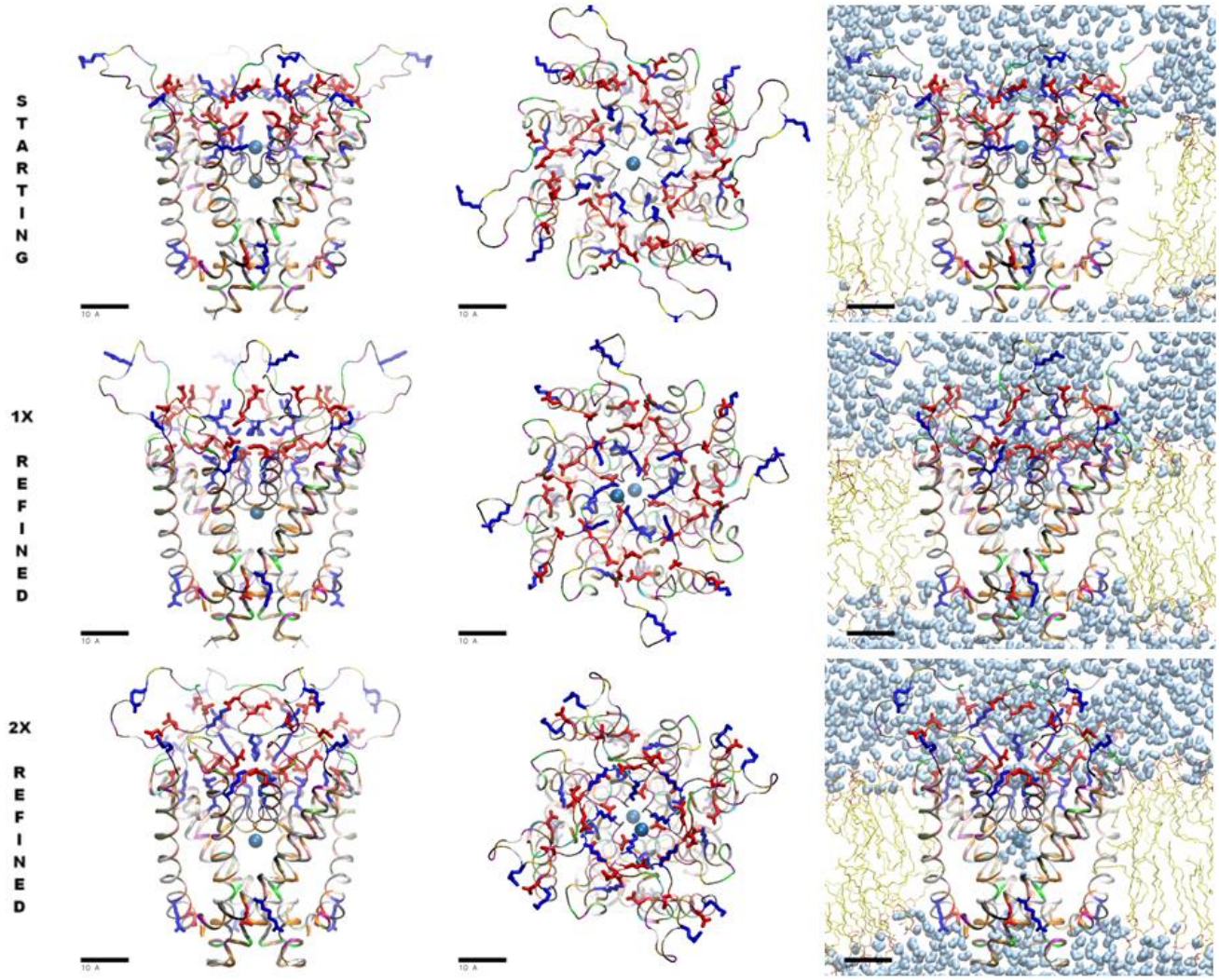

Supplementary Figure 13. Refinement of TRPV1 based structures
The TRPV1-based OSM-9 model was simulated with all the charged residues in the default dissociation state. Panels show progression of starting model through two cycles of refinement. Panels on the right show snapshot of refinement cycle tracking protein-lipid contacts, ion coordination, and hydration states. Protein backbone is colored by the residue name (Ala gray; Arg, Lys blue; Asn green; Asp, Glu red; Cys yellow; Gly black; Gln lime; His mauve; Ile, Leu white; Met orange; Phe pink; Pro cyan; Ser tan; Thr ochre; Trp, Tyr purple; Val silver).

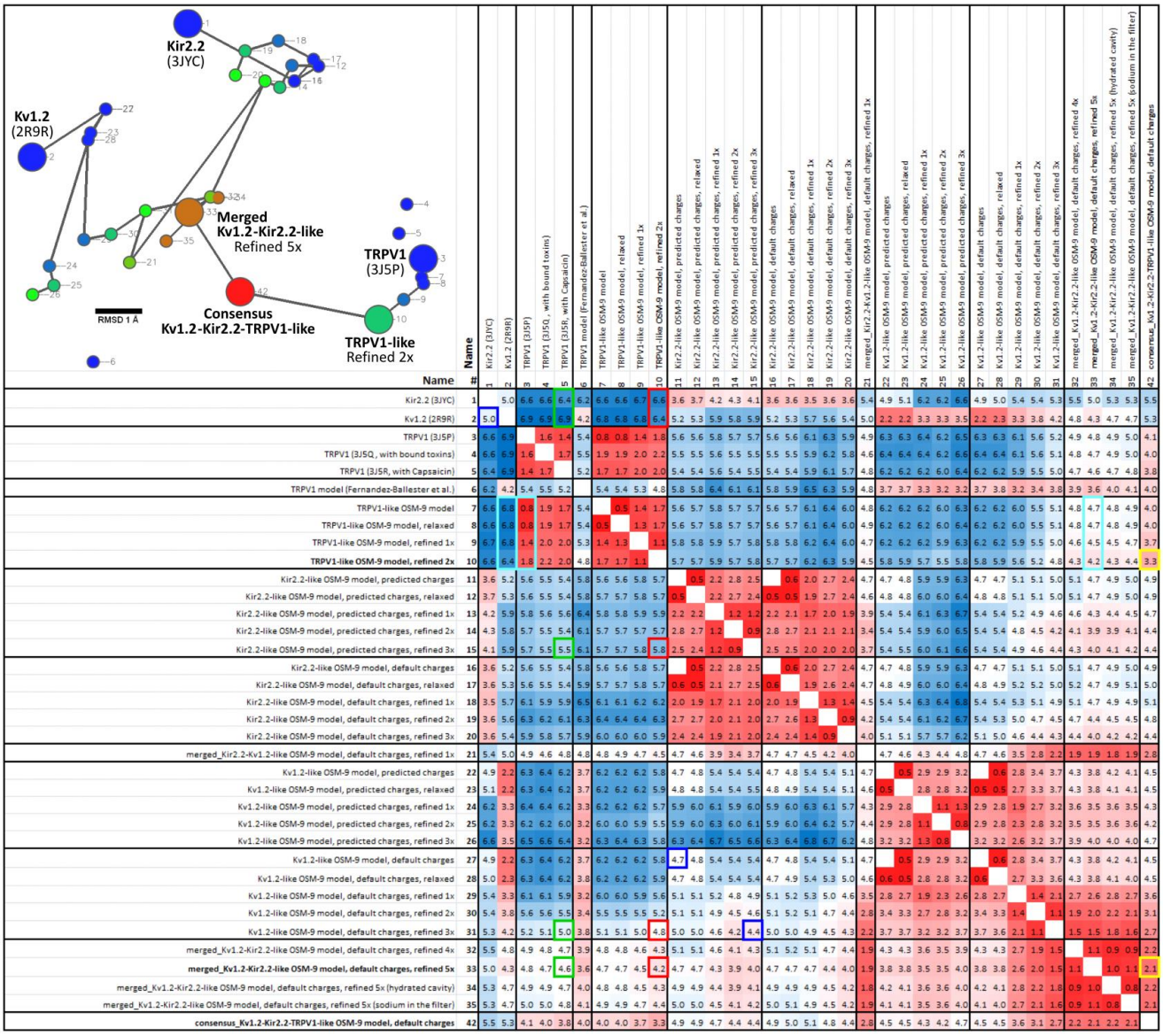

Supplementary Figure 14. Quantitative evaluation of RMSD between templates and models

This table depicts the structural comparison of the starting crystallographic templates[2-4], all major intermediate refinement steps (see Refinement Timeline), and three refined homology models of OSM-9. Root-Mean-Square Deviation (RMSD, in Å) was calculated for the homologous regions covering transmembrane helices S5 and S6, the pore helix and the selectivity filter. Refinement of Kir2.2- and Kv1.2-based models makes them more similar to the TRPV1 cryo-EM structure, comparing to the starting templates (green frames in the table). The Kir2.2- and Kv1.2-based models become more similar to each other during the independent cycles of the refinement (blue frames). Refinement of the TRPV1-based model drives structure away from TRPV1 template and towards the Kv1.2 template to certain extent (cyan frames) and makes it more similar to the refined Kv1.2-Kir2.2-like merged model (red frames). Slow convergence of the Kv1.2-Kir2.2-like merged model with the 2x refined TRPV1-based model to a continuously updated average produced a consensus model that is somewhat more similar to the Kv1.2-Kir2.2-like model rather than TRPV1-based model (yellow frames). An insert on the top left shows a 2D "map" reflecting pairwise structure similarity from RMSD table as spatial proximity. Structural comparison #6, potassium channel-based homology model of TRPV1 after[5].

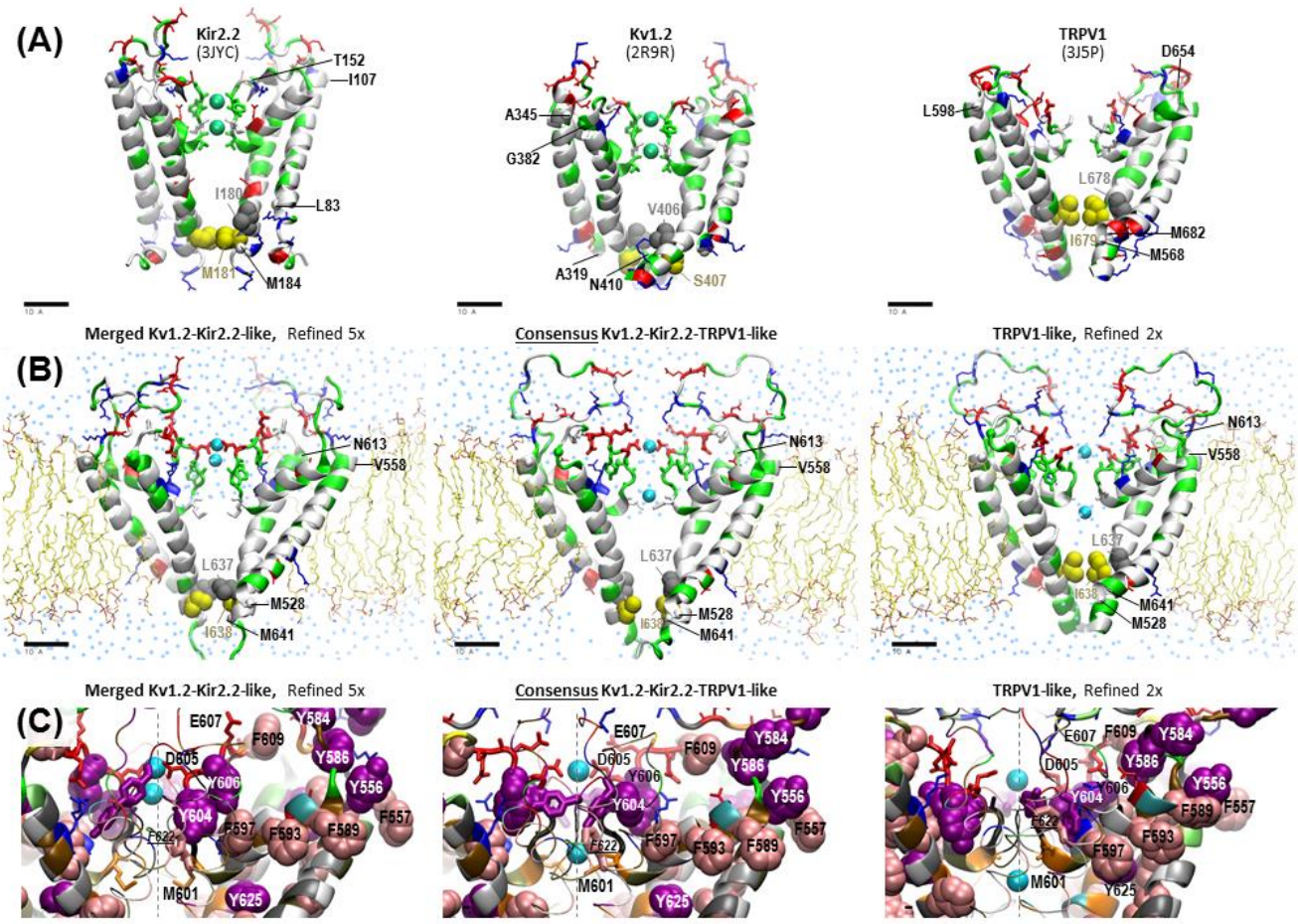

Supplementary Figure 15. Comparison of templates and targets

Row (A) Full-length view of the templates[2-4] used for building the homology models. Protein residues are colored by type (white – hydrophobic, green – hydrophilic, red – acidic, blue – basic). For Kir2.2 and Kv1.2 template structures two of the K^+ ions are shown in crystallographic positions as green spheres, they were replaced by Ca^{2+} ions in the homology models at the start of the refinement. As no ions were resolved in the cryo-EM TRPV1 structure, the Ca^{2+} ions in the homology models were originally placed above and below the narrowest part of the filter. The residues labeled in black on the panels in rows (A) and (B) mark the homologous positions for the beginning and the end of the transmembrane helices S5 and S6 in the starting OSM-9 models. The residues homologous to L637 and I638 (forming the hydrophobic gate in OSM-9 models) are shown in gray and yellow color respectively, in VDW representation. Row (B) Refined models based on Kv1.2-Kir2.2-like merged structures (left), TRPV1 (right), and the converged consensus model (center). A slice of water oxygens (cyan dots) through the simulation cell shows stably dehydrated ion chamber, while a continuous water pathway is retained in the selectivity filter of the refined Kv1.2-Kir2.2-like model and the consensus model, but not in TRPV1-based model. Row (C) Stacking in aromatic residues near the selectivity filter and the pore helix is shown for the three refined models. Side chains of tyrosines and phenylalanines are represented as purple and pink space fill respectively. Aromatic residues, shown as "thick licorice" rather than van der Waals are those that belong to another subunit, shown in front as thin tubes. Acidic and basic protein residues are colored red and blue respectively.

Supplementary Notes

Supplementary Note 1) Worm Behavior

In additional experiments, we assessed whether a mutation in this region can act in a dominant negative manner, when overexpressed in a WT background. Increasing concentrations of Y604G mutant DNA were injected into N2 WT worms to examine whether there is a dose-dependent effect. We observed no significant defects in osmotic avoidance behavior at all DNA concentrations tested (data not shown). Thus, the Y604G mutation is not capable of rendering channels that contain WT OSM-9 defective. It remains to be determined if this is due to the inability of the mutant to form multimers with WT OSM-9, or whether the presence of WT channel subunits confers WT behavior.

We also tested whether dampened osmotic avoidance behavior following starvation could be corrected by exposure to 5-hydroxytryptamine (5-HT), and whether this 5-HT effect could be attenuated by octopamine. We found reduced avoidance after starvation in OSM-9 WT rescue worms, increased avoidance in response to 5-HT, and reversal to after-starvation levels when worms were co-exposed to 5-HT and octopamine, following previously described methodology[8,9]. Again in striking contrast, Y604F worms did not show attenuation of the starvation response, did not show an increase of %-avoidance after exposure to 5-HT, and displayed unchanged %-avoidance in response to 5-HT/octopamine. These experiments suggest that modulation of osmotic avoidance behavior via defined molecular signaling mechanisms[8-10] depends on Ca^{2+} that enters the ASH nociceptor neuron via OSM-9.

Supplementary Note 2) Attempts to record electrophysiological data

Determined and resilient effort was spent to complement our *in vivo* Ca^{2+} imaging and behavioral data with channel physiology. For this, we first tried to record from OSM-9::GFP transfected cells, which were co-transfected with OCR-2, and then from cells transfected with a chimeric channel that had a TRPV4 backbone and transmembranes 5 through 6 from OSM-9, thus including OSM-9 pore helix and selectivity filter. Initial promising results were unfortunately inconsistent, despite repeated attempts and expression in different cell lines. The chimera was C-terminally fused to GFP so that channel expression and localization to the membrane could be verified (data not shown). Thus, we cannot provide electro-physiological data on ionic permeability for Y604F and Y606A.

Supplementary Note 3) Sequence analysis

We curated a set of 88 channel sequences from Genbank representative of TRPV sequences from various mammalian and invertebrate taxa and 1 TRPA1 sequence from a marine sponge, used as outgroup. These sequences were analyzed to assess the extent of primary amino acid sequence similarity between OSM-9, structural templates[1-4], and mammalian TRPV1-6 across pore forming regions (Supplementary Figure 1). Additionally, we assessed the conservation of secondary structure over individual channel subdomains (Supplementary Figure 2).

Amino acid secondary structure was predicted utilizing the algorithm JNet[11] implemented by Jalview v2.8[12]. JNet uses several different neural networks and decides on the most likely prediction via a jury network. Supplementary Figure 2A shows a multiple sequence alignment of secondary structural elements (amino acid letters encoded Helix, Extended, or Loop based on JNet classification). This course-grain alignment reveals that secondary structure is generally conserved across channel subtypes with insertion/deletions occurring primarily in loop regions between TM1 and TM2 and the turret region between TM5 and the pore helix. Panel B graphically depicts the secondary structure prediction of the TM5-TM6 region in OSM-9 by JNET, JHMM and JPSSM. Overall the predictions are similar and the subdomain boundaries of TM5 and TM6 largely agree with numerous transmembrane topology algorithms (not shown). Panel C shows a comparison of secondary structure assigned by the initial Kv1.2 or Kir2.2 template-based alignment, the initial 3D homology model, 3X refined, and 4x

refined and merged Kv1.2-Kir2.2-like OSM-9 model. These results show the assignment of secondary structure from homology modeling largely accords with other sequence based methods.

To estimate the degree of divergence between amino acid sequences we aligned the 88 channel sequences with Muscle [13,14] and parsed out the sequence regions representing individual channel subdomains (data not shown). We utilized MEGA5 [15] to quantify the number of amino acid differences per site between sequences with all ambiguous positions removed for each sequence pair. As one might expect we found that TM4, TM5, and TM6 are the most conserved subdomains in OSM-9, although they are still highly divergent. We limited the OSM-9 sequence boundaries between amino acids 523-649, encoding TM5-TM6 (i.e. the pore-forming unit). This estimation was informed by: (i) reported boundaries from previous TRP channel models, (ii) various predictions of secondary structure and transmembrane domain topology for OSM-9 and (iii) multiple sequence alignment of OSM-9 with the TRPV subfamily (main ms. Figure 7). Within the pore-forming unit we found a high degree of divergence with structural templates and TRP homologues. For example, we present the pairwise sequence alignment between structurally resolved KcsA[1] and TM5-TM6 of OSM-9 (Supplementary Figure 1). Specifically, we calculated the sequence identity for a variety of sequence fragments: TM5-TM6, percentage identity 10.7% (alignment length: 122 residues); Pore-Helix and Selectivity Filter, percentage identity 26.3% (19 residues); Selectivity Filter, percentage identity 42.9% (7 residues). In other comparisons, we quantified pairwise percentage identity between TM5-TM6 of OSM-9 versus Kv1.2 and Kir2.2 potassium channel templates and mouse versions of TRPV1-6 (Supplementary Figure 1B). Taken together, these data show a high degree of sequence divergence in the pore forming unit. Overall, these channels are much less conserved by primary amino acid sequence than by secondary structure, and presumably tertiary structure.

A main factor that determines the quality of a homology model is the alignment accuracy between template and target (Supplementary Figure 8-9). It is generally considered that the quality of the model stands questionable when the sequence identity falls in the twilight zone (<25-30% identity) of sequence similarity. In our case, both potassium channel templates are highly divergent: the Kir2.2, (3JYC) template and OSM-9 share sequence identity of 13.1%; the Kv1.2 (2R9R) template and OSM-9 share sequence identity of 12.3%; Kir2.2 (3JYC) and Kv1.2 (2R9R) share sequence identity of 20.35%. With respect to gaps in both Kv1.2 and Kir2.2 template-target alignments (Supplementary Figure 8), insertions/deletions in one are mostly absent in the other. While the overall percentage identity in the alignment of OSM-9 against either structure is low, there are several regions with significant blocks of similarity. Previous reports also found low identity alignments between TRP and potassium channel templates in a similar range of identity and similarity[5,16-18]**.**
Based upon the low degree of sequence identity we took extra care in all analyses and refinement steps to try and achieve the highest level of precision one could expect given the divergence.

Since OSM-9 and other TRP channels have low sequence identity (<25% id) to potassium channel templates, conclusions based solely on these homology models should be taken with a grain of salt. However, quite recently, three cryo-EM structures of rat TRPV1 (PDB: 3J5P, 3J5Q, and 3J5R) were reported with crystallographic resolution 3.3, 3.8, and 4.2 Å respectively [4]. Pairwise sequence identity between OSM-9 and 3J5Q is shown in Supplementary Figure 9 (~31% id with turret removed). These new structural references are less divergent from OSM-9 compared to Kv1.2 and Kir2.2. These structures afford us the novel opportunity to generate, refine, and quantitatively compare homology models of OSM-9 based upon potassium channel templates and the new TRPV1 channel templates.

Supplementary Note 4) Homology modeling
As described above, we utilized the structurally resolved potassium channel Kv1.2-2.1 Paddle Chimera Channel (PDB ID: 2R9R), the chicken inward-rectifier potassium channel Kir2.2 (PDB ID: 3JYC), and TRPV1 cryo-EM structures (PDB ID: 3J5P) as templates [2-4]. The TRPV1 and Kv1.2

monomers possess six transmembrane domains while the full length Kir2.2 monomer contains only two transmembrane domains. For all templates and the OSM-9 target, four monomers combine to form the channel pore domain. One rationale for the use of multiple templates is based on our desire to track any variation in orientation, conformation or match to the membrane environment that may indicate higher quality of one model over the other. Both Kv1.2 and Kir2.2 templates used in this paper have a comparable degree of sequence divergence to OSM-9. However they have certain differences in orientation and position of the transmembrane helices. In addition, similar to OSM-9, Kir2.2 structure has a turret region, which was removed in TRPV1 and absent in Kv1.2, and was modeled *de-novo* for those templates. Turrets have been structurally resolved in multiple potassium channels [2] and the presence of a turret in OSM-9 is consistent with recent reports modeling turrets in TRPV channels and their potential role in temperature sensation [18,19].

We used MODELLER (9v8) [20-22] to generate 30 initial models of OSM-9 based on Kv1.2 or Kir2.2 templates or based on the three TRPV1 cryostructures. MODELLER uses a variety of methods (e.g. Z-DOPE, molpdf, GA341) to assess the model. These scores are associated with the estimated accuracy of the model [23]; the molpdf and DOPE scores can be used to rank models. Supplementary Figure 10A reports the model assessment scores for all template-based models used in this study (molpdf, lower values are considered better models; DOPE scores, the lower values are considered better models; Z-score, positive scores are likely to be poor models, whereas scores lower than -1 or so are likely to be native; Procheck, a good quality model would be expected to have over 90% of residues in the most favoured region, Ramachanran Plot). Overall, the unliganded (3J5P) TRPV1-based starting structure has the best model assessment scores. Specifically, it has the lowest Z-DOPE score (0.44) of all models. We chose to refine this TRPV1-based model and compare it with refinements of the top candidate model from each potassium channel template.

4.1) Generation of tetramers representing the putative pore-forming unit

For each monomer (Kv1.2- or Kir2.2-based), one hundred candidate symmetrical tetramer models were generated using SYMMDOCK which predicts multimers using a geometry-based docking algorithm [24,25]. SYMMDOCK predicts the cyclically symmetric complex given the input symmetric unit structure and the symmetry order 'n' (n =4 tetramer). The algorithm produces top hundred cyclically symmetric transformations in both its search and clustering by exploiting local feature matching. We visually inspected each tetramer and selected the best models whose domain organization accords to both Kv1.2 and Kir2.2 templates and previous TRP channel models [5,16-18,26,27]. The criteria included the tightness of the inter-subunit contacts, the width of the conductive pathway, and the expected match to the lipid bilayer. For the TRPV1-based monomer we spatially aligned the structure over the TRPV1 cryo-EM template in VMD using the minimal deviation of the homologous helical regions as criterion to generate the putative tetramer for refinement.

4.2) Molecular Dynamic simulations

We implemented a refinement strategy using iterative cycles of unrestrained simulation and symmetry-driven annealing in explicit media. In this manner we can derive important information about the hydration of the protein and ions, dynamics of the ions in the filter, interaction of the channel with lipids, de-wetting of the hydrophobic gate and partial de-wetting of the ion chamber. These MD simulations and annealing refine models through interactions with the medium and provided informed, detailed and reliable insight into a model's quality and stability (see Supplementary Figure 10B for simulation protocol).

To perform the MD Simulations, we used the NAMD package[28]. Assembly of the simulation cells, analysis and visualization of the results were performed using custom written Tcl scripts in VMD v1.9.1 [29]. All MD Simulations were performed in the NPT ensemble using CHARMM36 [30,31] force field parameters and TIP3P water model[32]. The acidic and basic residues were set in two variants for each

model: one variant in their default protonation state, and another (marked as “Kir2.2-like, predicted charges” and “Kv1.2-like, predicted charges” on Supplementary Figure 10B (refinement protocol). For the latter two structures the dissociation state of the ionizable residues was estimated using PROPKA for the neutral pH[33].

Based on that, residues D^{605}, and K^{619} for Kir2.2-derived model and E^{591}, D^{605}, E^{607}, E^{608}, and K^{619} for Kv1.2-derived model were set non-dissociated. The N- and C-termini were set to a truncated non-dissociated state since the real protein is longer than the simulated fragment in both directions. All the models were embedded in a POPE (1-[(2)H(31)] palmitoyl-2-oleoyl-sn-glycero-3-phosphoethanolamine) bilayer membrane (pre-equilibrated for 40 ns in the Laboratory of Molecular & Thermodynamic Modeling (PI Jeffery Klauda), University of Maryland, College Park) surrounded by water, 247 and 228 POPE molecules for simulations with Kv1.2 and Kir2.2 templates respectively.

The presence and the location of cations might significantly influence the structure of the selectivity filter [34, 35, 36]. Two Ca^{2+} ions were placed in the filter in two (S1 and S3) out of four positions found in the template crystal structures. Two water molecules were placed in the remaining two positions, alternating with the Ca^{2+} ions. To maintain the electroneutrality of the system Na^+ and Cl^- ions were added up to equivalent of 150 mM salt concentration – 52 Na^+ and 48 Cl^- for all Kir2.2-based systems, 64 Na^+ and 72 Cl^- for Kv1.2-based system with PROPKA-predicted dissociation states, and 68 Na^+ and 64 Cl^- for Kv1.2-based system with default protonation. Langevin Dynamics [37,38] was used to maintain constant pressure (1 atm) and constant temperature (303.15^o K) in a flexible simulation cell to allow relaxation of the in-plane area. Periodic boundary conditions were maintained and the particle mesh Ewald method[39] with a real space cutoff distance of 12 Å and a grid width of 0.97 Å. Energy Minimization steps were performed using the steepest descent in the first 2000 steps and then a conjugate gradient in the subsequent 2000 steps. To attain the equilibrium, the system was subjected to gradual heating until it reached to 303.15^{o}K (30^{o}C), first with the protein backbone harmonically restrained (1 kcal/mol/A^2 per backbone atom) to the initial coordinates, while the lipids were allowed to pack around and water to stably solvate the protein for 5 ns.

Since in the TRPV1 cryo-EM structures no ions were resolved, in the starting TRPV1-based model we have placed the Ca^{2+} ions manually, based on similarity of ion placement in potassium channels in the vicinity of the pore-facing backbone oxygens of the filter (Supplementary Figure 13). In the TRPV1-based model it is much shorter, which limits the number of possible positions for an ion. Importantly, the side chains of D^{605} in the starting model are facing away ("upwards") from the filter, they are not sufficiently close to coordinate ions to a reasonable degree. Unlike the highly selective potassium channels, where the filter is tight and K^+ ions are stripped of most of the hydration shell, a low-selective filter as in OSM-9 is likely to allow Ca^{2+} ions to keep most of the hydration shell, and therefore is probably wider and more dynamic.

As a family, TRP channels are generally considered non-selective cation channels. Hence, one might expect that the filters in these channels be sufficiently flexible to accommodate ions of multiple sizes (Pauling radii/pm: K^+, 133; Na^+, 95; Ca^{2+}, 99; Mg^{2+}, 65) and differential hydrations states of the ion (e.g. Ca^{2+} can have up to 9 H_20 molecules in its first hydration layer). In support of this, it has been shown that TRPV1 and TRPV5 channels have wide pores and dilate in the presence of agonists. Furthermore, the kinetics of pore widening demonstrates a dependence of the rate of widening as a function of solute radius [40,41]. Therefore, the position of the ions in such a filter is probably not very restricted and might allow certain degree of freedom - they do not necessarily have to be exactly at the pore axis. Along the permeation pathway, more energetically favorable positions at some steps might be near the acidic side chains. Because of that, we did not put any restraints on the position of the ions during the refinement process (i.e. only the protein is symmetry-restrained).

4.3) Confining ions to the vicinity of the selectivity filter

Starting imprecision in the modeled conformation of the selectivity filter region might cause the loss of coordinated ions at the beginning of the unrestrained simulation, which in turn might distort the filter conformation and hinder its refinement. To avoid this, we have used Tcl scripting in NAMD to apply soft boundary conditions for ions that would prevent them from leaving the 12 Å vicinity of the center of mass of the selectivity filter, but do not apply any force within this sphere. The boundary conditions were present through all the simulations, however the ions were found to settle at the binding points within the filter after the first few nanoseconds of simulation and after that did not attempt to leave the selectivity filter and did not approach the boundary, therefore no forces were applied to ions through the most of the simulation time.

4.4) Symmetry-driven simulated annealing

To refine the channel structure in an explicit all-atom medium and study the network of protein-protein, protein-lipid, and protein-ion interactions across the channel, we applied a simulation protocol that combines cycles of unrestrained relaxation with a recently developed symmetry-restrained annealing step. Previous results have shown that unrestrained simulations are useful in refining small and medium size proteins but have limited competency in improving the refinement of larger low-resolution models [42,43]. When compared to unrestrained models alone, symmetry-restrained annealing has been shown to improve accuracy (by up to 50%) in homology models of potassium channels [44].

In the symmetry-driven simulated annealing protocol, a rotational symmetric average conformation is calculated for the four monomers composing OSM-9 channel. A weak harmonic force (spring constant starting at 0.001 kcal/mol/Å^2) is applied to every atom of a monomer to drive it slowly towards the symmetric average. The average is continuously updated (every 10 fs), so that the final conformation is not pre-defined at the beginning, but is gradually "chosen" by the system. One of the principles underlying the refinement is that if one of the monomers finds a more stable conformation than others, then driving all of them to symmetric average will prompt the unstable monomers to change first and adopt the more stable conformation. The strength of the harmonic restraints gradually increases to produce near-linear decrease in RMS deviation of the structure from symmetric average (at start it is usually on the order of a few Å) over 1 ns annealing simulation.

Supplementary Figure 10B depicts the protocol employed for the molecular dynamic refinement for all simulations that were conducted for this study. In total, we simulated more than 154 ns of molecular dynamics for the OSM-9 pore. From the initial TRPV1-based starting model we implemented two cycles of 5ns relaxation and 1 ns annealing each with default charges for the ionization state. From the initial starting models (Kv1.2- and Kir2.2-based) we implemented three cycles of 5 ns relaxation and 1 ns annealing. These simulations were repeated for two different ionization states- default charges and PROPKA-predicted[33] charges. After performing three cycles of 5 ns relaxation and 1 ns annealing we re-analyzed the dissociation state of amino acids in the Kv1.2- and Kir2.2-based models using PROPKA3 [33]. Unlike the starting conformation, all the residues (including the residues D^{605}, and K^{619} for Kir2.2-derived model and E^{591}, D^{605}, E^{607}, E^{608}, and K^{619} for Kv1.2-derived model that were simulated non-dissociated) were estimated to have their default dissociation at neutral conditions. This fact likely indicates that the starting unconventional dissociation state was reflecting some minor conflicts in the starting conformation rather than the essential features of the modeled structures.

For all the subsequent relaxation/annealing cycles we simulated the default dissociation state for the Kv1.2- and Kir2.2-based models. Nevertheless, using two alternative dissociation sets have provided certain benefits: the analysis of the quality of the refined models indicates that the OSM-9 structure based on Kir2.2 with the predicted charges ranks higher than structure based on Kir2.2 with the default dissociation state. One can speculate that in some conditions varying the dissociation state of amino acids can be useful for exploring the conformational space of the models as it can allow the

structure to temporarily overcome energy barriers not possible in the default dissociation state (e.g. if the charged residue is trapped in a “wrong” salt bridge or needs to switch from one hydrophilic pocket to another through a hydrophobic region).

4.5) Comparative analyses of single-template OSM-9 models

We assessed refinements to the TRPV1-, Kv1.2- and Kir2.2-based starting structures through comparative analyses of protein-lipid contacts and hydration states between structures and cycles of the simulation (Supplementary Figures 11-13). Specifically, by tracking the distribution of water molecules in the vicinity of the channel, one can identify potential structural issues that need to be resolved such as leaking chamber walls, leaking filter, and streams of water between helices. Conversely, the lack (or repair) of issues through cycles of refinement may give confidence to a particular structure over another.

All four variants (default and predicted dissociation states of Kv1.2- and Kir2.2-based models) pull significant amount of water into the region near the selectivity filter. In the Kv1.2-based models at the first stage of refinement water spontaneously forms and maintains a few strings through the gate region; however, by the second refinement both Kv1.2-based models "evolve" to eliminate water strings in the hydrophobic gate. Initially in one of the Kv1.2-based models with a dissociated K^{619}, water tends to form strings in the space between S5 and S6 helices, either to the cytoplasmic or external sites, although during the second refinement K^{619} repositions more closely to the hydrated region near the selectivity filter and water strings interrupt. We observe that the channel chamber seems to be easily dehydrated in the absence of ions; however, presence of even one Ca^{2+} ion holds water in the chamber.

The Kir2.2-based models have a different hydration pattern. These models initially show strings of water crossing the S6 bundle from the chamber to the periplasmic bulk side. Notably, this negative feature was not completely eliminated in future refinements. A point of distinction between Kir2.2- and Kv1.2-based models is that the putative gate region seems to be more tightly closed in Kir2.2-based models. Comparatively, the Kv1.2-based OSM-9 models appear to be more stable, both in transmembrane helices and the loops. In this model, the selectivity filter is positioned somewhat higher than the Kir2.2-based structure; however, the Kv1.2-based filter is about at the same height as it was after the very first annealing. Notably, both structures have ions in similar positions and coordinations.

Taken together, these simulations show that the initial Kv1.2- and Kir2.2-based starting models had some minor structural issues such as leaking chamber walls, leaking filter, water strings between helices 5 and 6, and exposure of some polar residues to the lipids. The fact that the simulation protocol employed solved most of them demonstrates that symmetry-driven annealing improves the quality of the models rather than just testing them in simulations. With respect to the turret in the Kv1.2-based model, there is still a conflict even after three cycles of simulation. In the initial starting model the turret is largely unstructured and sticks straight up into the extracellular media. After three cycles of refinement the turret has become more compact and perpendicular to the membrane; however, its loops erroneously cross in an impossible conformation. Conversely, the turret in the Kir2.2-based model was more structured and compact in the initial starting structure versus the model after the third cycle of refinement. Hence there is a tendency for the turret to be extended in both models. Merging the models helped resolve turret issues, see below.

For the TRPV1-based starting structure, we found the ion chamber to be narrow even at start, and the water content of the ion chamber not to increase (Supplementary Figure 13). As in our Kv1.2- and Kir2.2-based models it tended to dehydrate. The fit to the membrane is reasonably good and there is no water permeation between the channel and the lipids. The gate is dry. These features indicate that

the starting model is of suitable good quality. However, a more troublesome feature in the starting TRPV1-based model is the filter which quickly collapsed (flattened) in simulation; it is also dry in the very middle. Conversely, our Kv1.2- and Kir2.2-based models had a stable water string and ion presence in the middle of the filter. The TRPV1-based structure is derived from a channel with higher % sequence identity – yet still highly divergent. One of the reasons the filter in the simulated TRPV1-based model, which shows several advantageous features, is collapsed and apparently non-conductive could be that the template is a cryo-EM structure. The filter region in a native structure is probably well hydrated and water is a critical structural element. Low temperature might affect the aggregate state of water and therefore, likely alter the structure of the filter region in a cryo-structure.

In the 1x refined TRPV1-based model the top Ca^{2+} ion stays at the side, near two D^{605} side chains, while the lower ion is close to symmetry axis being coordinated by four partial charges of backbone oxygens. Further improvements are seen in the 2x refined TRPV1-based model. Ca^{2+} ions stay in similar positions where they were after the first round - above and below the filter. After the unrestrained stage we observe a continuous string of water in the filter, however after symmetry annealing the filter has de-wetted again. The filter got narrower compared to the previous cycle. Some of the charged residues in the loops have aggregated in a salt-bridged ring-like structure, an interesting conformation. These salt-bridges pulled the top of the channel together to a narrower conformation.

4.6) Converging two models to a single "consensus" conformation

After each cycle of refinement, we manually inspected each model to assess stability and any differences that may inform preferences to one model over the other. After three rounds of refinement the two best Kv1.2- and Kir2.2-based models were selected based on structural fitness criteria. The dissociation state of the ionizable side chains was re-evaluated using PROPKA and found to be the default dissociation for the neutral pH for both models.

Importantly, even before the models were merged, we found that in the course of refinement cycles both models were converging towards a common structure to a certain extent (Supplementary Figure 14). Only after convergence had leveled off did we apply our protocol for gradual steering two alternative models towards a common conformation. Similar to symmetry-driven annealing, an instantaneous average of the two structures was computed and the soft harmonic forces were applied to every protein atom towards continuously updated average to ensure gradual convergence over 1 ns. Since more stable regions will persist longer than unstable regions in the presence of a small uniform force, the merged model tends to combine the most stable features of the two starting models.

After converging the Kv1.2- and Kir2.2-based models together, we performed two cycles of relaxation/annealing. In addition, we conducted a cycle of refinement with either a hydrated cavity, Na^+ in the filter, or mutations to aromatic tyrosine residues at amino acid positions 604 or 606 (Supplementary Figure 12). The wild-type channel structures obtained after the five simulations (Supplementary Figure 10B) can be considered as the most promising potassium channel-based models of OSM-9, in slightly different states - the top one has the driest inner cavity, the second one is more hydrated (although with less water than was added at the beginning of the simulation cycle; there is certainly some tendency towards dehydration in this model), and the third one has Na^+ ions in the selectivity filter, which organizes it to some extent. Notably, the strings of water crossing the S6 bundle from the chamber to the periplasmic bulk side in the 3x refined Kir2.2-based model have been corrected in the merged model (Supplementary Figure 11). In addition, conflict in the turret from the 3x refined Kv1.2-based model has been resolved in the Kv1.2-Kir2.2-like merged structure though it is still extended and largely unstructured. Nevertheless, we observe dynamic motion in the turret and changes in the extent of hydration in the different conformations it adopts.

Notably, we also found that in the course of refinement the TRPV1-based model spontaneously "evolved" from the initial TRPV1 conformation to become closer to the refined Kv1.2-Kir2.2-like merged model. Specifically, this change occurred in overall structure and particularly in the way Ca^{2+} ions are coordinated by acidic side chains at the filter entrance. Hence, we also conducted one final simulation - merging the 2x refined TRPV1-based model and our 5x refined Kv1.2-Kir2.2-like merged model together to a consensus conformation. In this way we addressed which structural features will dominate. For quantitative evaluation of the entire set of homology models we calculated root-mean-square deviation (RMSD in Å, lower number indicates better superimposition) for backbone atoms of superimposed protein regions. These analyses represent the transmembrane helices, pore helix and selectivity filter derived from comparison of the potassium channel templates, TRPV1 EM cryo-structures, a published TRPV1 model based on a potassium channel template [5], and starting and refined models of OSM-9 from the current work. We compared more than 36 structures, four channel regions in different combinations (S5, S6, pore helix and filter) totaling thousands of pairwise comparisons (Supplementary Figure 14).

With this metric, our best potassium channel-based model is the final merged and refined Kv1.2-Kir2.2-like structure with the dry pore. It approaches the closest with the structure 3J5R (TRPV1 with bound capsaicin), with RMSD 4.6 Å. Other expectations about the course of model refinement are supported by these RMSD data. For example, OSM-9 models from both Kv1.2 and Kir2.2 templates approach the TRPV1 cryo-EM structure in the course of refinement; Kir2.2- and Kv1.2-based OSM-9 models start at 6.6 and 6.9 Å from 3J5R, respectively, and refine down to 5.5 and 5.0 Å respectively. They also approach each other - starting at 5.0 Å from each other, they converge down to 4.4 Å. Importantly, merging them together again increases model accuracy, evidenced by a decrease of RMSD from the TRPV1 cryo-EM structure from 5.5 and 5.0 Å, down to 4.6 Å. Overall, the comparative values in the table are quite encouraging: they show that in the course of refinement the TRPV1-based model becomes more similar to our 5x refined Kv1.2-Kir2.2-like merged model. Inversely, the TRPV1-based models become less similar to the starting TRPV1 conformation. Specifically, before we merged the TRPV1- and Kv1.2-Kir2.2-like models together, the RMSD distance between them was 4.2 Å. The resulting consensus model ended up being more similar to the merged Kv1.2-Kir2.2-like model - 2.1 Å, vs. 3.3 Å from the TRPV1-based 2x-refined model. Taken together, these data increase our confidence that the refinement methods are working and that models are progressing in the right direction.

One discrepancy between the 5x refined Kv1.2-Kir2.2-like merged model and the TRPV1-based model is that, in the former, the S6 helix is positioned one turn lower, towards the cytoplasmic/gate side (see residues L^{637} and I^{638}, Supplementary Figure 15). This difference might have caused the narrowing of the upper gate-forming ring of the isoleucines in our Kv1.2-Kir2.2-like model. However, one cannot say that the shift of S6 is necessarily wrong - one can imagine such a variation in two family members such as TRPV1 and OSM9. Indeed TRPV1 is likely to show critical structural differences from OSM-9 since it is unable to rescue osmotic avoidance behavior in worms but can confer *de-novo* capsaicin sensitivity[45]. Remarkably, in the process of refinement of the TRPV1-based model, the S6 helix shifted downwards, more similar to the Kv2.1/Kir2.2-based model. The S6 helix shifted even lower in the consensus structure, after converging TRPV1- and Kv1.2-Kir2.2-like models together, which agrees with the suggestion that the position of S6 might be the most stable in the Kv1.2-Kir2.2-like models.

4.7) Comparisons to newly resolved TRPV1 cryo-EM structure

Supplementary Figure 15 depicts OSM-9 models versus template structures. Compared to the TRPV1 cryostructure, the 5x refined Kv1.2-Kir2.2-like merged model correctly predicts the start and end of pore-lining TM domains, their axial rotation (i.e. what side looks into the pore), overall tilt, and the pore

helix. This model also successfully identified the residues comprising the gate region, with only minor differences, and "second gate" region positioned right under the filter formed by methionine in both channels. The acidic residues above the filter form a similar negative funnel. In both channels the filter seems to be wide enough to path the ions with most of the hydration shell, hence the low selectivity. The wider filter in TRPV1 templates versus the OSM-9 Ca^{2+}-in-filter model may not necessarily be a structural feature that differentiates OSM-9, but a function of the degree to which divalent cations are coordinated in the cryo-preparations. Notably, in the refined Kv1.2-Kir2.2-like merged model that has Na^{+} ions present instead of Ca^{2+} the filter is exactly as wide as the one in TRPV1 structure 3J5Q.

4.8) Effect of dehydration on structural confirmation

With respect to the effect of dehydration on local or global conformation, the structural changes associated with the hydration of the pore are rather minor. As indicated in the protocol, we have hydrated the de-wetted cavity of the refined model and then performed one more cycle of 5 ns unrestrained simulation followed by 1 ns symmetry annealing for both dry and hydrated versions. Comparison of the backbone of the helical parts (transmembrane helices and P-helix) shows deviation with RMSD of only 0.88 Å. The main change in conformation is the gate region becoming somewhat more compact and tall in the hydrated model - possibly prompted by the surface tension of the water droplet in the cavity, at the level of P^{630}. It slightly increases the tilt of the pore-lining helices and effectively displaces the position of the ion chamber and filter towards the external side by ~0.7 Angstrom. The only noticeable change in the side chain arrangement in the cavity is that in the dry chamber the "second gate" formed by M^{601} under the filter has Methionine side chains coming together, while in the hydrated version they swing open to the side, thus allowing a water string connecting the filter and water droplet in the chamber.

Supplementary Note 5) Selectivity Filter aromatic residues

When considering the impact of residues Y^{604}, Y^{606}, and F^{609} on the selectivity filter we also examined them in the context of the homology models. In these models it appears that residues with large hydrophobic side chains are critical to pore geometry, and therefore ion permeability. We found that Y^{604} plays an important role in ion selectivity, which is demonstrated by the complete elimination of Ca^{2+} influx into ASH for the Y604F mutation. Yet ASH is still activated in Y604F mutant worms, albeit not fully to WT levels. It is well established that tyrosine residues are critical contributors to the Kv channel selectivity signature sequence, defined as TXXTXGYG. TRPV1-6 channels do not typically have tyrosine residues in their predicted selectivity filters[46,47], although invertebrate TRPV channels are replete with aromatics in the presumed selectivity filters (main ms. Figure 7). We find it attractive to hypothesize that Y^{604} could function in a manner similar to that of the tyrosine residue in Kv channels and serve a structural role in maintaining the orientation of the filter. This concept is in keeping with our homology modeling data (Supplementary Figure 15 and Supplementary Movie).

The finding that mutation of Y604F partially maintains the worm's avoidance behavior indicates that the aromatic ring at position 604 is important to pore geometry. Y^{604} could possibly function as a master scaffold via its aromatic side chain. This concept implies that Y^{604} is at the core of the OSM-9 selectivity filter and could influence the local positions of residues D^{605}, Y^{606}, and E^{607}, among others. The aromatic ring and hydroxyl group of the tyrosine residue facilitates Ca^{2+} permeation. The aromatic ring without the hydroxyl group is more hydrophobic and does not allow Ca^{2+} to permeate, so that presumably only sodium can enter the cell. Changing the charge landscape of the pore by removing the hydroxyl group from the aromatic ring leads to reduced Ca^{2+} permeability, but not Na^{+} permeability, allowing for partial activation of ASH. In that case, Na^{+} mediated depolarization would be the activation mechanism of ASH that drives the appreciable avoidance behavior of Y604F worms.

Modeling data also suggest that the aromatic side chain of F^{609} is not a pore lining residue *per se*, but may contribute significantly to the size and hydration of the pore and have a considerable range of

motion in various channel conformations. Integrating our experimental data and computational modeling, we propose that mutations of aromatic residues that drastically alter both behavior and Ca^{2+} influx (Y^{604} and F^{609}) are amino acids that are critical to pore geometry. Alterations to pore geometry invariably result in changes to ion permeability. This can be further extended in future molecular dynamics studies.

Supplementary References

1. Uysal, S.*, et al.* Crystal structure of full-length KcsA in its closed conformation. *Proc Natl Acad Sci U S A* 106, 6644-6649 (2009).

2. Tao, X., Avalos, J.L., Chen, J. & MacKinnon, R. Crystal structure of the eukaryotic strong inward-rectifier K+ channel Kir2.2 at 3.1 A resolution. *Science* 326, 1668-1674 (2009).

3. Long, S.B., Tao, X., Campbell, E.B. & MacKinnon, R. Atomic structure of a voltage-dependent K+ channel in a lipid membrane-like environment. *Nature* 450, 376-382 (2007).

4. Cao, E., Liao, M., Cheng, Y. & Julius, D. TRPV1 structures in distinct conformations reveal activation mechanisms. *Nature* 504, 113-118 (2013).

5. Fernandez-Ballester, G. & Ferrer-Montiel, A. Molecular modeling of the full-length human TRPV1 channel in closed and desensitized states. *J Membr Biol* 223, 161-172 (2008).

6. Kaplan, J.M. & Horvitz, H.R. A dual mechanosensory and chemosensory neuron in Caenorhabditis elegans. *Proc Natl Acad Sci U S A* 90, 2227-2231 (1993).

7. Liedtke, W., Tobin, D.M., Bargmann, C.I. & Friedman, J.M. Mammalian TRPV4 (VR-OAC) directs behavioral responses to osmotic and mechanical stimuli in Caenorhabditis elegans. *Proc Natl Acad Sci U S A* 100 Suppl 2, 14531-14536 (2003).

8. Mills, H.*, et al.* Monoamines and neuropeptides interact to inhibit aversive behaviour in Caenorhabditis elegans. *Embo J* 31, 667-678 (2012).

9. Harris, G.*, et al.* The monoaminergic modulation of sensory-mediated aversive responses in Caenorhabditis elegans requires glutamatergic/peptidergic cotransmission. *J Neurosci* 30, 7889-7899 (2010).

10. Hapiak, V.*, et al.* Neuropeptides amplify and focus the monoaminergic inhibition of nociception in Caenorhabditis elegans. *J Neurosci* 33, 14107-14116 (2013).

11. Cole, C., Barber, J.D. & Barton, G.J. The Jpred 3 secondary structure prediction server. *Nucleic Acids Res* 36, W197-201 (2008).

12. Waterhouse, A.M., Procter, J.B., Martin, D.M., Clamp, M. & Barton, G.J. Jalview Version 2--a multiple sequence alignment editor and analysis workbench. *Bioinformatics* 25, 1189-1191 (2009).

13. Edgar, R.C. MUSCLE: a multiple sequence alignment method with reduced time and space complexity. *Bmc Bioinformatics* 5, 1-19 (2004).

14. Edgar, R.C. MUSCLE: multiple sequence alignment with high accuracy and high throughput. *Nucleic Acids Research* 32, 1792-1797 (2004).

15. Tamura, K.*, et al.* MEGA5: molecular evolutionary genetics analysis using maximum likelihood, evolutionary distance, and maximum parsimony methods. *Molecular biology and evolution* 28, 2731-2739 (2011).

16. Grandl, J.*, et al.* Pore region of TRPV3 ion channel is specifically required for heat activation. *Nature neuroscience* 11, 1007-1013 (2008).

17. Liu, C.H.*, et al.* In vivo identification and manipulation of the Ca2+ selectivity filter in the Drosophila transient receptor potential channel. *J Neurosci* 27, 604-615 (2007).

18. Yang, F., Cui, Y.Y., Wang, K.W. & Zheng, J. Thermosensitive TRP channel pore turret is part of the temperature activation pathway. *Proceedings of the National Academy of Sciences of the United States of America* 107, 7083-7088 (2010).

19. Ryu, S., Liu, B., Yao, J., Fu, Q. & Qin, F. Uncoupling proton activation of vanilloid receptor TRPV1. *J Neurosci* 27, 12797-12807 (2007).

20. Eswar, N.*, et al.* Comparative protein structure modeling using MODELLER. *Current protocols in protein science / editorial board, John E. Coligan ... [et al.]* Chapter 2, Unit 2 9 (2007).

21. Marti-Renom, M.A.*, et al.* Comparative protein structure modeling of genes and genomes. *Annual review of biophysics and biomolecular structure* 29, 291-325 (2000).

22. Sali, A. & Overington, J.P. Derivation of rules for comparative protein modeling from a database of protein structure alignments. *Protein Sci* 3, 1582-1596 (1994).

23. Eramian, D., Eswar, N., Shen, M.Y. & Sali, A. How well can the accuracy of comparative protein structure models be predicted? *Protein Sci* 17, 1881-1893 (2008).

24. Schneidman-Duhovny, D., Inbar, Y., Nussinov, R. & Wolfson, H.J. Geometry-based flexible and symmetric protein docking. *Proteins* 60, 224-231 (2005).

25. Schneidman-Duhovny, D., Inbar, Y., Nussinov, R. & Wolfson, H.J. PatchDock and SymmDock: servers for rigid and symmetric docking. *Nucleic Acids Research* 33, W363-W367 (2005).

26. Poteser, M.*, et al.* PKC-dependent coupling of calcium permeation through transient receptor potential canonical 3 (TRPC3) to calcineurin signaling in HL-1 myocytes (vol 108, pg 10556, 2011). *Proceedings of the National Academy of Sciences of the United States of America* 108, 13876-13878 (2011).

27. Nilius, B.*, et al.* The selectivity filter of the cation channel TRPM4. *The Journal of biological chemistry* 280, 22899-22906 (2005).

28. Phillips, J.C.*, et al.* Scalable molecular dynamics with NAMD. *Journal of computational chemistry* 26, 1781-1802 (2005).

29. Humphrey, W., Dalke, A. & Schulten, K. VMD: visual molecular dynamics. *Journal of molecular graphics* 14, 33-38, 27-38 (1996).

30. A. D. MacKerell, D.B., Bellott, R. L. Dunbrack, J. D. Evanseck, M. J. Field, S. Fischer, J. Gao, H. Guo, S. Ha, D. Joseph-McCarthy, L. Kuchnir, K. Kuczera, F. T. K. Lau, C. Mattos, S. Michnick, T. Ngo, D. T. Nguyen, B. Prodhom, W. E. Reiher, B. Roux, M. Schlenkrich, J. C. Smith, R. Stote, J. Straub, M. Watanabe, J. Wiórkiewicz-Kuczera, D. Yin, M. Karplus. All-Atom Empirical Potential for Molecular Modeling and Dynamics Studies of Proteins. *J. Phys. Chem. B* 102, 3586-3616 (1 April 1998).

31. Klauda, J.B.*, et al.* Update of the CHARMM all-atom additive force field for lipids: validation on six lipid types. *The journal of physical chemistry* 114, 7830-7843 (2010).

32. William L. Jorgensen, J.C., Jeffry D. Madura, Roger W. Impey, and Michael L. Klein. Comparison of simple potential functions for simulating liquid water. *J. Chem. Phys.* 79, 10 (1983).

33. Rostkowski, M., Olsson, M.H., Sondergaard, C.R. & Jensen, J.H. Graphical analysis of pH-dependent properties of proteins predicted using PROPKA. *BMC structural biology* 11, 6 (2011).

34. Zhou, Y., Morais-Cabral, J.H., Kaufman, A. & MacKinnon, R. Chemistry of ion coordination and hydration revealed by a K+ channel-Fab complex at 2.0 A resolution. *Nature* 414, 43-48 (2001).

35. Bhate, M.P., Wylie, B.J., Tian, L. & McDermott, A.E. Conformational dynamics in the selectivity filter of KcsA in response to potassium ion concentration. *Journal of molecular biology* 401, 155-166 (2010).

36. Berneche, S. & Roux, B. A gate in the selectivity filter of potassium channels. *Structure* 13, 591-600 (2005).

37. Glenn J. Martyna, D.J.T., Michael L. Klein. Constant pressure molecular dynamics algorithms. *The Journal of Chemical Physics* 101, 4177-4189 (1994).

38. Scott E. Feller1, Y.Z., Richard W. Pastor1, and Bernard R. Brooks. Constant pressure molecular dynamics simulation: The Langevin piston method. *J. Chem. Phys.* 103, 9 (1995).

39. Darden, T.Y., Darrin; Pedersen, Lee. Particle mesh Ewald: An N . log(N) method for Ewald sums in large systems. *The Journal of Chemical Physics* 98, 4 (1993).

40. Chung, M.K., Guler, A.D. & Caterina, M.J. TRPV1 shows dynamic ionic selectivity during agonist stimulation. *Nature neuroscience* 11, 555-564 (2008).

41. Yeh, B.I., Kim, Y.K., Jabbar, W. & Huang, C.L. Conformational changes of pore helix coupled to gating of TRPV5 by protons. *Embo J* 24, 3224-3234 (2005).

42. Chen, J. & Brooks, C.L., 3rd. Can molecular dynamics simulations provide high-resolution refinement of protein structure? *Proteins* 67, 922-930 (2007).

43. Fan, H. & Mark, A.E. Refinement of homology-based protein structures by molecular dynamics simulation techniques. *Protein science : a publication of the Protein Society* 13, 211-220 (2004).

44. Anishkin, A., Milac, A.L. & Guy, H.R. Symmetry-restrained molecular dynamics simulations improve homology models of potassium channels. *Proteins* 78, 932-949 (2010).

45. Tobin, D.*, et al.* Combinatorial expression of TRPV channel proteins defines their sensory functions and subcellular localization in C. elegans neurons. *Neuron* 35, 307-318 (2002).

46. Owsianik, G., Talavera, K., Voets, T. & Nilius, B. Permeation and selectivity of TRP channels. *Annual review of physiology* 68, 685-717 (2006).

47. Heginbotham, L., Lu, Z., Abramson, T. & MacKinnon, R. Mutations in the K+ channel signature sequence. *Biophysical journal* 66, 1061-1067 (1994).